JCI insight

Deficiency of *Socs3* leads to brain-targeted EAE via enhanced neutrophil activation and ROS production

Zhaoqi Yan, … , Hongwei Qin, Etty N. Benveniste

JCI Insight. 2019. https://doi.org/10.1172/jci.insight.126520.

Research In-Press Preview **Inflammation**

Dysregulation of the JAK/STAT signaling pathway is associated with Multiple Sclerosis (MS) and its mouse model, Experimental Autoimmune Encephalomyelitis (EAE). Suppressors Of Cytokine Signaling (SOCS) negatively regulate the JAK/STAT pathway. We previously reported a severe, brain-targeted, atypical form of EAE in mice lacking *Socs3* in myeloid cells ($Socs3^{\Delta LysM}$), which is associated with cerebellar neutrophil infiltration. There is emerging evidence that neutrophils are detrimental in the pathology of MS/EAE, however, their exact function is unclear. Here we demonstrate that neutrophils from the cerebellum of $Socs3^{\Delta LysM}$ mice show a hyper-activated phenotype with excessive production of reactive oxygen species (ROS) at the peak of EAE. Neutralization of ROS in vivo delayed the onset and reduced severity of atypical EAE. Mechanistically, *Socs3*-deficient neutrophils exhibit enhanced STAT3 activation, a hyper-activated phenotype in response to G-CSF, and upon G-CSF priming, increased ROS production. Neutralization of G-CSF in vivo significantly reduced the incidence and severity of the atypical EAE phenotype. Overall, our work elucidates that hypersensitivity of G-CSF/STAT3 signaling in $Socs3^{\Delta LysM}$ mice leads to atypical EAE by enhanced neutrophil activation and increased oxidative stress, which may explain the detrimental role of G-CSF in MS patients.

Deficiency of *Socs3* Leads to Brain-targeted EAE via Enhanced Neutrophil Activation and ROS Production

Zhaoqi Yan[1], Wei Yang[1], Luke Parkitny[1], Sara A. Gibson[2], Kevin S. Lee[1], Forrest Collins[1], Jessy S. Deshane[3], Wayne Cheng[4], Amy S. Weinmann[4], Hairong Wei[1], Hongwei Qin[1]* and Etty N. Benveniste[1]*

[1]Department of Cell, Developmental and Integrative Biology, University of Alabama at Birmingham, Birmingham, Alabama, USA; [2]Lineberger Comprehensive Cancer Center, University of North Carolina at Chapel Hill, Chapel Hill, North Carolina, USA; and Departments of [3]Medicine and [4]Microbiology, University of Alabama at Birmingham, Birmingham, Alabama, USA.

***Co-Corresponding Authors:**

Dr. Hongwei Qin, Department of Cell, Developmental and Integrative Biology, University of Alabama at Birmingham, 1918 University Boulevard, MCLM 390, Birmingham, AL 35294. Phone: +1-205-934-2573. E-mail address: hqin@uab.edu

Dr. Etty (Tika) Benveniste, Department of Cell, Developmental and Integrative Biology, University of Alabama at Birmingham, 510 20th Street South, 1220 Faculty Office Tower, Birmingham, AL 35294. Phone: +1-205-934-7667. E-mail address: tika@uab.edu

Conflict of Interest Statement

The authors have declared that no conflict of interest exists.

Abstract

Dysregulation of the JAK/STAT signaling pathway is associated with Multiple Sclerosis (MS) and its mouse model, Experimental Autoimmune Encephalomyelitis (EAE). Suppressors Of Cytokine Signaling (SOCS) negatively regulate the JAK/STAT pathway. We previously reported a severe, brain-targeted, atypical form of EAE in mice lacking *Socs3* in myeloid cells (*Socs3*$^{\Delta LysM}$), which is associated with cerebellar neutrophil infiltration. There is emerging evidence that neutrophils are detrimental in the pathology of MS/EAE, however, their exact function is unclear. Here we demonstrate that neutrophils from the cerebellum of *Socs3*$^{\Delta LysM}$ mice show a hyper-activated phenotype with excessive production of reactive oxygen species (ROS) at the peak of EAE. Neutralization of ROS *in vivo* delayed the onset and reduced severity of atypical EAE. Mechanistically, *Socs3*-deficient neutrophils exhibit enhanced STAT3 activation, a hyper-activated phenotype in response to G-CSF, and upon G-CSF priming, increased ROS production. Neutralization of G-CSF *in vivo* significantly reduced the incidence and severity of the atypical EAE phenotype. Overall, our work elucidates that hypersensitivity of G-CSF/STAT3 signaling in *Socs3*$^{\Delta LysM}$ mice leads to atypical EAE by enhanced neutrophil activation and increased oxidative stress, which may explain the detrimental role of G-CSF in MS patients.

Introduction

Multiple Sclerosis (MS) is an autoimmune disease that affects the central nervous system (CNS) (1). The disease causes severe demyelination and neuronal loss in both the brain and spinal cord, which leads to neurological dysfunction, including visual loss, limb weakness, ataxia and impaired cognition (2, 3). Although there are 15 FDA approved disease-modifying therapies, none is able to stop disease progression (3). The pathobiology of MS is very complex and both innate and adaptive immunity contribute to disease development and progression (4). Experimental Autoimmune Encephalomyelitis (EAE) is a widely used mouse model of MS mediated by autoimmune $CD4^+$ T-cells and cells of the innate immune system (5). Clinical and histopathological similarities between MS and EAE allow findings obtained from the EAE model to be extrapolated to patients with MS.

Neutrophils are the most abundant cell type in human blood and are the first responders of the immune system when the body encounters foreign antigens or sterile inflammation (6, 7). Neutrophils initiate immune responses by secretion of pro-inflammatory cytokines/chemokines, degranulation, generation of reactive oxygen species (ROS), formation of neutrophil extracellular traps (NETs), and antigen presentation (6, 8-10). Neutrophils are involved in the pathology of CNS autoimmune diseases such as MS/EAE and Neuromyelitis Optica Spectrum Disorder (NMOSD) (11-15). Neutrophils contribute to EAE disease by secretion of pro-inflammatory cytokines (16, 17), promoting maturation of antigen-presenting cells such as dendritic cells and macrophages (18) and disruption of the blood-spinal cord-barrier (19). Neutrophil

related chemokines/mediators (G-CSF, CXCL1, CXCL8, CXCL5 and neutrophil elastase) correlate with neurological disability and lesion burden in MS patients (20). Neutrophils from MS patients exhibit a primed, hyper-activated phenotype compared to healthy controls (21). Moreover, several studies indicate that administration of G-CSF, the cytokine that is critical for maturation of neutrophils, leads to MS relapses (22, 23). NMOSD is an autoimmune demyelinating disease distinct from MS, characterized by optic neuritis, astrocytopathy and serum antibodies against Aquaporin-4 (24). Neutrophils are prominent in CNS lesions and cerebrospinal fluid (CSF) from NMOSD patients (25). Indeed, CSF from NMOSD patients induces neutrophil chemotaxis and activation, resulting in astrocyte activation to a pro-inflammatory phenotype (26). G-CSF also plays a detrimental role in patients with NMOSD (27).

The JAK/STAT signaling pathway plays a critical role in activation and regulation of immune responses (28). Dysregulation of the JAK/STAT pathway is associated with many pathological conditions, including MS (29, 30). We previously demonstrated that inhibition of the JAK/STAT pathway ameliorates disease severity in a number of EAE models (31). STAT3 has been identified as an MS susceptibility gene (32, 33) and hyper-activation of STAT3 is observed in peripheral blood mononuclear cells (PBMC) from MS patients and correlates with disease progression (34). Suppressors Of Cytokine Signaling (SOCS) are a family of proteins that negatively regulate the JAK/STAT pathway (35). SOCS3 inhibits activation of STAT1 and STAT3, thereby terminating signaling through this pathway (36-38). Reduced SOCS3 expression has been observed in PBMCs from MS patients during relapses, which correlates with

enhanced STAT3 activation (39). In NMOSD, clinical benefit has been observed with anti-IL-6R antibody treatment (40). The deleterious role of IL-6 is speculated to be mediated, in part, by IL-6 expansion of Th17 cells (41, 42), which occurs through a STAT3-dependent mechanism (43).

There are different phenotypes of EAE, including classical and atypical. Classical EAE is characterized by ascending paralysis with preferential immune cell infiltration in the spinal cord (5). Atypical EAE is associated with brain inflammation and characterized by ataxia and tremors. Some EAE models display a mixed phenotype of both classical and atypical clinical symptoms. We previously reported that deficiency of *Socs3* in myeloid cells (*Socs3*$^{\Delta LysM}$) leads to a severe, non-resolving atypical form of EAE (44, 45). Specifically, this brain-targeted atypical EAE is dependent on preferential neutrophil infiltration in the cerebellum (44). However, the exact mechanism by which neutrophils induce atypical EAE is not clear. Here we demonstrate that neutrophils from *Socs3*$^{\Delta LysM}$ mice produce excessive amounts of ROS, which is critical for the brain-targeted atypical EAE phenotype. Furthermore, neutrophils lacking *Socs3* are hyper-sensitive to G-CSF priming, which leads to enhanced oxidative burst in response to pro-inflammatory cytokines, and *in vivo,* G-CSF depletion significantly reduces atypical EAE disease progression. Overall, our findings demonstrate the importance of *Socs3* in controlling the hyper-activation of neutrophils, and add to our understanding on the role of neutrophils in MS/EAE.

Results

***Socs3*$^{\Delta LysM}$ Mice Exhibit Brain-targeted EAE With Infiltration of Hyper-activated Neutrophils.** *Socs3*$^{\Delta LysM}$ mice with atypical EAE exhibit non-resolving ataxia and tremor, along with preferential cerebellar neutrophil infiltration (44, 45). We assessed demyelination in this model using Black Gold staining, revealing that *Socs3*$^{\Delta LysM}$ mice exhibit cerebellar demyelination at the peak of EAE disease, whereas *Socs3*$^{fl/fl}$ mice retain intact myelin structure in the cerebellum (**Fig. 1A**).

Neutrophils have been implicated in both spinal cord-targeted, classical EAE (19, 20, 46, 47), as well as brain-targeted, atypical EAE (44, 48-50), although there is controversy about their exact functions. To address the role for neutrophils in atypical EAE, we first determined levels of surface receptors on cerebellar-infiltrating neutrophils using multi-color flow cytometry analysis (**Supplemental Fig. 1**). The cerebellar-infiltrating neutrophils in *Socs3*$^{\Delta LysM}$ mice exhibit increased surface levels of CD11b and CXCR4 compared to *Socs3*$^{fl/fl}$ mice, while surface levels of CD62L and CXCR2 were decreased in *Socs3*$^{\Delta LysM}$ mice compared to *Socs3*$^{fl/fl}$ mice (**Figs. 1B and 1C**). This altered surface marker expression profile has been associated with a primed neutrophil phenotype (6, 51-53). Primed neutrophils exhibit characteristics that include increased chemotaxis, increased degranulation, and enhanced production of ROS, and these phenotypes are observed in autoimmune conditions (52, 54). Consistent with a phenotype of increased chemotaxis, we found that the numbers of cerebellar neutrophils were significantly increased in *Socs3*$^{\Delta LysM}$ mice at the peak of EAE (**Fig. 1D**). CD63 is a membrane protein associated with intracellular granules. During degranulation, CD63 is expressed

on the cell surface as the granule membrane and cell membrane merge (55). Analysis of surface expression of CD63 revealed that neutrophil degranulation was also increased in *Socs3*$^{\Delta LysM}$ mice at the peak of EAE (**Fig. 1E**).

We next assessed whether ROS production was altered in *Socs3*$^{\Delta LysM}$ mice. To measure total ROS production, neutrophils isolated from the cerebellum were incubated with CM-H2DCFDA, a chemically reduced form of fluorescein used as an ROS indicator in live cells (18, 56). This revealed an increase in the level of ROS^{+} neutrophils in the cerebellum at the peak of EAE in *Socs3*$^{\Delta LysM}$ mice (**Fig. 1F**). ROS production also increased on a per cell basis, as measured by an increase in the mean fluorescence intensity (MFI) of CM-H2DCFDA staining (**Figs. 1G and 1H**). To determine if neutrophils were the primary source of oxidative burst in the cerebellum of *Socs3*$^{\Delta LysM}$ mice, ROS production was measured in neutrophils, monocytic cells, microglia and other leukocytes. As shown in **Fig. 1I**, neutrophils produce the highest levels of ROS amongst these cell populations. Amongst all the species of free radicals, superoxide produced via NADPH Oxidase 2 (NOX2) is considered harmful to endothelial cells and has detrimental roles in CNS inflammation (57-59). We measured superoxide by DHE and consistent with total ROS levels, superoxide was also increased in cerebellar neutrophils from *Socs3*$^{\Delta LysM}$ mice **(Fig. 1J)**. To determine oxidative stress in *Socs3*$^{\Delta LysM}$ mice, we measured the expression of *Hmox1*, a gene induced by ROS (60) in whole cerebellar tissue. Consistent with enhancement of oxidative stress, *Hmox1* mRNA expression was increased at the peak of EAE in *Socs3*$^{\Delta LysM}$ mice compared to *Socs3*$^{fl/fl}$ mice **(Fig. 1K)**. Together, these results demonstrate that brain-targeted, atypical EAE

pathology in *Socs3*$^{\Delta LysM}$ mice is correlated with a primed neutrophil phenotype and enhanced ROS production.

ROS Plays Important Roles in the Pathology of Brain-targeted EAE. We next determined whether oxidative stress contributes to the brain-targeted EAE phenotype. To neutralize ROS, we administered a cocktail of ROS scavengers to *Socs3*$^{\Delta LysM}$ mice seven days after immunization (56). Administration of ROS scavengers significantly delayed the time of onset and reduced the severity of brain-targeted EAE (**Fig. 2A**). The incidence of brain-targeted EAE was also reduced (92.9% to 47.1%) **(Table 1).** Administration of ROS scavengers also prevented demyelination in the cerebellum (**Fig. 2B**).

To better understand the underlying mechanism associated with the beneficial effect of ROS scavengers in atypical EAE, we assessed immune cell infiltration in mice treated with the ROS scavenger cocktail. At days 13-14, we observed a significant reduction in neutrophils, monocytic cells and $CD3^+$ T-cells infiltrating the cerebellum in mice treated with ROS scavengers, however, the frequency of microglia was comparable between Vehicle Control and ROS scavenger treatment (**Fig. 2C**). *Hmox1* mRNA expression was significantly reduced in the cerebellar tissues from mice treated with ROS scavengers, indicating an overall reduction of oxidative stress (**Fig. 2D**)**.** To exclude the possibility that treatment with the ROS scavenger cocktail suppresses atypical EAE by affecting T-cell priming, we determined the frequency of MOG-specific T-cells after treatment. The frequency of MOG-specific T-cells, determined by either cytokine production upon MOG

stimulation (**Supplemental Fig. 2A**) or MOG_{38-49} tetramer staining (**Supplemental Figs. 2C and 2D**), were comparable between ROS scavenger treatment and Vehicle Control. The percentage of regulatory T-cells after ROS scavenger treatment was also not changed (**Supplemental Fig. 2B**).

Socs3$^{\Delta LysM}$ mice can exhibit classical EAE in addition to the predominant atypical EAE phenotype. There was not a significant change in the incidence or severity of classical EAE upon ROS scavenger treatment **(Table 1, Supplemental Fig. 2E)**, indicating that the impact of ROS scavengers was specific to brain-targeted EAE. Collectively, these results demonstrate that ROS play a critical role in the development of brain-targeted atypical EAE, but not in classical spinal cord-targeted EAE.

G-CSF Treatment Promotes a Primed Phenotype in *Socs3*-deficient Neutrophils via JAK1/STAT3. We next explored the mechanism underlying the primed neutrophil phenotype. SOCS3 negatively regulates STAT3 signaling and is induced upon activation of the JAK/STAT pathway (61). Therefore, we first determined which cytokines induce *Socs3* expression in neutrophils. Activation of STAT3 by G-CSF in neutrophils has been well documented (37, 62-64), however, the literature is inconclusive about whether other cytokines such as IL-6 and IL-23 can activate neutrophils via STAT3 (65, 66). We found that G-CSF treatment induced strong *Socs3* expression 2 h after stimulation, and that this response was significantly higher than that induced by other cytokines such as IL-6 and IL-23 (**Fig. 3A**). In addition, G-CSF treatment led to enhanced STAT3 activation in *Socs3*-deficient neutrophils, in

comparison to *Socs3*$^{fl/fl}$ neutrophils (**Figs. 3B and 3C**). This difference was not observed in response to IL-6 (**Figs. 3B and 3C**) or IL-23 (**Supplemental Figs. 3A and 3B**). We previously reported that loss of *Socs3* leads to persistent STAT3 activation in response to IFN-γ stimulation in bone marrow-derived macrophages (36). However, in neutrophils, treatment with IFN-γ induced only moderate expression of *Socs3* compared to treatment with G-CSF (**Fig. 3A**), and IFN-γ treatment did not lead to enhanced STAT3 activation in *Socs3*-deficient neutrophils *in vitro* (**Supplemental Figs. 3C and 3D**).

Upon G-CSF stimulation, *Socs3*-deficient neutrophils exhibited a primed phenotype *in vitro*, evident as increased surface expression of CD11b and CXCR4, and decreased surface expression of CD62L and CXCR2 relative to *Socs3*$^{fl/fl}$ neutrophils (**Figs. 3D and 3E**). In contrast, this difference for CD11b or CD62L was not observed upon stimulation with other cytokines, including IFN-γ, IL-17A/F, IL-6, IL-6 + sIL-6R, IL-23 or IL-6 + IL-23 (**Supplemental Fig. 3E**). We next asked whether the primed phenotype was due to activation of the JAK/STAT pathway. Pre-treatment of *Socs3*-deficient neutrophils with AZD1480, a JAK1/2 inhibitor, or PF8041, a JAK1 inhibitor, impaired G-CSF-induced neutrophil priming (**Fig. 3F**). These results indicate that G-CSF treatment activates the JAK1/STAT3 pathway to elicit a primed phenotype in *Socs3*-deficient neutrophils *in vitro*.

G-CSF Induces a Unique Gene Expression Profile in *Socs3*-deficient Neutrophils. We next determined whether G-CSF stimulation differentially affects gene expression in *Socs3*-deficient neutrophils. RNA-seq analysis was performed on *Socs3*$^{fl/fl}$ or *Socs3*-

deficient neutrophils that were either un-stimulated or stimulated with G-CSF. G-CSF stimulation impacted the expression of a large number of genes in both *Socs3*$^{fl/fl}$ and *Socs3*-deficient neutrophils, with more than 2000 genes significantly up- or down-regulated after stimulation (**Fig. 4A**). Moreover, a total of 873 genes were up-regulated, and 939 genes down-regulated, specifically in *Socs3*-deficient neutrophils compared to *Socs3*$^{fl/fl}$ neutrophils (**Fig. 4B**).

A gene set enrichment analysis (GSEA) revealed that a number of signaling pathways related to neutrophil activation were enhanced in *Socs3*-deficient neutrophils as compared to *Socs3*$^{fl/fl}$ neutrophils upon G-CSF stimulation (**Fig. 4C**). Up-regulated pathways included the NF-κB pathway, which is related to neutrophil activation and chemotaxis in response to TNF-α and Toll-like Receptor (TLR) ligands (67), and the STAT5 pathway, which is critical for neutrophils to response to GM-CSF (68). Not surprisingly, STAT3 signaling was also up-regulated in *Socs3*-deficient neutrophils upon G-CSF stimulation compared to *Socs3*$^{fl/fl}$ neutrophils. G-CSF mobilizes neutrophils by promoting chemotaxis, and our RNA-seq data indicate that neutrophil migration-related genes were increased in *Socs3*-deficient neutrophils treated with G-CSF (**Figs. 4C and 4D**). Additionally, by qRT-PCR analysis, we confirmed that chemokines which promote neutrophil migration, including *Ccl4*, *Cxcl2* and *Cxcl3*, were also enhanced in *Socs3*-deficient neutrophils compared to *Socs3*$^{fl/fl}$ neutrophils **(Fig. 4E)**. The RNA-seq analysis also indicated that expression of genes related to the secretory vesicle trafficking pathway were increased in *Socs3*-deficient neutrophils, consistent with an increased potential for degranulation (**Figs. 4C and 4D**). In contrast, many of the down-regulated

pathways in *Socs3*-deficient neutrophils were associated with neutrophil resolution, including IFN-α responses (**Fig. 4C**). DNA replication and protein translation related pathways were also reduced in *Socs3*-deficient neutrophils, indicating a maturation stage (**Fig. 4C**).

To further determine whether G-CSF stimulated *Socs3*-deficient neutrophils are more activated as compared to $Socs3^{fl/fl}$ neutrophils, we performed enrichment analysis using previously published RNA-seq gene sets that contain genes expressed by activated neutrophils (stimulated with live bacteria, LPS or TNF-α) (51, 69, 70). Genes that were increased by such activated neutrophils overlapped extensively with genes that were significantly up-regulated in *Socs3*-deficient neutrophils upon G-CSF stimulation (**Supplemental Fig. 4**). In addition, genes that were reduced after stimulation from the published data overlap extensively with down-regulated genes in *Socs3*-deficient neutrophils upon G-CSF stimulation (**Supplemental Fig. 4**). Overall, the results from the RNA-seq analysis indicate that upon G-CSF stimulation, *Socs3*-deficient neutrophils up-regulate neutrophil activation genes and down-regulate neutrophil resolution-related genes.

***Socs3*-deficient Neutrophils are Functionally Hyper-activated *In Vitro* upon G-CSF Priming**. Based on the results in **Fig. 3** and the RNA-seq data in **Fig. 4**, we hypothesized that *Socs3*-deficient neutrophils are more sensitive to priming by G-CSF. To test this hypothesis, we first assessed ROS production by neutrophils using a luminol-based assay. For this assay, bone marrow neutrophils were pre-incubated with

G-CSF overnight, followed by stimulation with PMA. In contrast to the expectation of our hypothesis, the data indicated that ROS production was comparable between *Socs3*$^{fl/fl}$ and *Socs3*-deficient neutrophils (**Fig. 5A**).

The RNA-seq results indicated the possibility that the NF-κB and STAT5 pathways were activated upon G-CSF priming of *Socs3*-deficient neutrophils **(Fig. 4C)**. Therefore, we next tested whether *Socs3*-deficient neutrophils were more sensitive to cytokines utilizing the NF-κB and STAT5 pathways. TNF-α and GM-CSF are pro-inflammatory cytokines produced by T-cells and myeloid cells in MS/EAE, and neutrophils are responsive to both cytokines (67, 68). Additionally, TNF-α- and GM-CSF-mediated induction of ROS plays a detrimental role during neuroinflammation by disrupting the blood-brain-barrier (BBB) (71, 72). To test the role for these cytokines in ROS induction, we treated neutrophils with TNF-α (**Fig. 5B**) or GM-CSF (**Fig. 5C**) after priming with G-CSF overnight. In the presence of PMA, both cytokines induced higher production of ROS in *Socs3*-deficient neutrophils, as compared to *Socs3*$^{fl/fl}$ neutrophils. The G-CSF primed *Socs3*-deficient neutrophils also showed increased degranulation upon LPS stimulation compared to *Socs3*$^{fl/fl}$ neutrophils (**Fig. 5D**). Together, these results indicate that *Socs3*-deficient neutrophils become hyper-activated *in vitro* upon G-CSF priming.

G-CSF Neutralization Ameliorates Brain-targeted EAE by Preventing Neutrophil Infiltration and Hyper-activation. Our results indicate that G-CSF leads to a primed phenotype in *Socs3*-deficient neutrophils *in vitro* and that this phenotype correlates with the incidence of brain-targeted EAE. Therefore, we next examined whether depleting G-

CSF is beneficial for brain-targeted EAE. We first examined the levels of G-CSF during EAE, which revealed that G-CSF levels were lower in the plasma of *Socs3*$^{\Delta LysM}$ mice compared to *Socs3*$^{fl/fl}$ mice at pre-onset of EAE and were comparable throughout the onset stage and peak of EAE **(Supplemental Fig. 5A)**. The levels of G-CSF in the cerebellum were comparable between *Socs3*$^{\Delta LysM}$ mice and *Socs3*$^{fl/fl}$ mice **(Supplemental Fig. 5B)**. Next, we determined whether G-CSF depletion affected the development and/or phenotype of EAE. In previous studies, we found that neutrophils migrated into the spleen and lymph nodes throughout the course of EAE in both *Socs3*$^{fl/fl}$ and *Socs3*$^{\Delta LysM}$ mice (data not shown). To avoid affecting the possible influence of neutrophils at the T-cell priming stage, anti-G-CSF Ab was administered to mice beginning on day 7 post-immunization. Administrating neutralizing Ab to G-CSF significantly reduced the levels of G-CSF in plasma (**Fig. 6A**). Depletion of G-CSF significantly reduced the severity (**Fig. 6B**) and incidence (**Table 2**) of brain-targeted EAE, and reduced cerebellar demyelination (**Fig. 6C**). A flow cytometry analysis indicated that G-CSF depletion significantly reduced the frequencies of infiltrating neutrophils and monocytic cells at the peak of EAE, while the frequencies of microglia and infiltrating $CD3^+$ T-cells were unchanged (**Fig. 6D**).

The reduced cerebellar infiltration (**Fig. 6D**) correlated with a significant reduction in the frequency of neutrophils and monocytes that were present in the blood after G-CSF depletion (**Supplemental Figs. 6A and 6B**). In contrast, the frequency of $CD3^+$ T-cells present in the blood were not altered (**Supplemental Fig. 6B**). Furthermore, the reduction of neutrophils in the blood did not affect neutrophil frequency in the spleen

(**Supplemental Fig. 6C**), suggesting a preferential reduction of CNS infiltration. Consistent with the significant reduction of infiltrating neutrophils in the cerebellum, the overall levels of oxidative stress were decreased, indicated by the reduction of ROS-producing neutrophils in the cerebellum (**Fig. 6E**) and significantly reduced *Hmox1* mRNA expression in the cerebellar tissues **(Fig. 6F).** Neutrophil degranulation was also reduced in the cerebellum (**Fig. 6G**). Interestingly, we did not observe a significant change in the incidence of classical EAE (**Table 2**) or disease severity (**Supplemental Fig. 7A**). G-CSF neutralization did reduce infiltration of neutrophils in the spinal cord, whereas the infiltration of microglia, monocytic cells and $CD3^+$ T-cells was not affected (**Supplemental Fig. 7B**). However, the change in neutrophil infiltration did not affect disease incidence or severity. Collectively, these results indicate that G-CSF neutralization ameliorates brain-targeted EAE by reducing neutrophil hyper-activation.

Discussion

We and others have demonstrated that brain-targeted, atypical EAE is predominantly a neutrophil-driven disease (11, 13, 44, 48, 49, 73, 74). Previously, we reported that neutrophils increase production of pro-inflammatory cytokines, chemokines, and nitric oxide during onset of atypical EAE in *Socs3*$^{\Delta LysM}$ mice (44). In the present study, we have elucidated the cellular mechanisms by which neutrophils induce pathological changes in the cerebellum of *Socs3*$^{\Delta LysM}$ mice. We demonstrated that neutrophils from the cerebellum of *Socs3*$^{\Delta LysM}$ mice exhibit a hyper-activated phenotype and increase ROS production, which contributes to the development of atypical EAE. Mechanistically, we found that neutrophil hyper-activation is mediated by enhanced G-CSF signaling through the JAK/STAT pathway in *Socs3*-deficient neutrophils. Consistent with these results, we demonstrated that G-CSF neutralization has beneficial effects in brain-targeted, atypical EAE. These findings contribute to our understanding of the pathobiology of brain-targeted EAE and document the detrimental role of neutrophils in autoimmune neuroinflammation.

Recent studies suggest that neutrophils are quite heterogeneous and comprise different subsets with distinct functions (6, 75, 76). Zhang et al., reported a unique subset of “aged” neutrophils characterized by high expression of CXCR4 and low expression of CD62L (51). These aged neutrophils represent an overly activated subset of neutrophils that were associated with increased pro-inflammatory activity and enhanced ROS production. Hawkins et al., reported that in a B-cell dependent classical EAE model, CNS-infiltrating neutrophils specifically express the adhesion molecule ICAM1 (46).

These ICAM1^{+} neutrophils exhibit increased surface expression of CD11b and CD45, form synapses with T-cells and B-cells, and mediate inflammatory responses *in vivo*. These findings suggest that expression of specific neutrophil surface markers could be associated with distinct functions. In the current study, *Socs3*-deficient, hyper-activated neutrophils exhibit alterations in surface marker expression (elevated CD11b and CXCR4, decreased CD62L and CXCR2), enhanced ROS production, and increased degranulation both *in vivo* (**Fig. 1**) and *in vitro* (**Figs. 3 and 5**). These results are consistent with clinical evidence showing that neutrophils from MS patients are characterized by increased TLR2 expression, elevated degranulation, resistance to apoptosis, and enhanced NET and ROS production, indicative of a hyper-activated status (21, 25).

The role of neutrophils in MS and EAE is complex. A number of studies, including from our group, indicate that neutrophils have detrimental functions in EAE (20, 44, 46-49, 77). Neutrophil depletion significantly reduces the incidence and severity of atypical EAE (44). Furthermore, mice lacking G-CSF signaling are resistant to classical EAE, and neutrophil-related chemokine levels correlate with MS lesion burden (20). In addition, overexpression of CXCL1 in the CNS increases neutrophil infiltration and exacerbates demyelination in two mouse models of MS, and neutrophil ablation reduced the severity of demyelination, demonstrating a pathogenic role for neutrophils (47, 77). However, a recent study showed polymorphonuclear myeloid-derived suppressor cells (PMN-MDSCs) restrain accumulation of GM-CSF producing B-cells in the CNS, exerting a protective effect in classical EAE (78). Depletion of PMN-MDSCs

after the onset of EAE led to activation of B-cells in the CNS, subsequent microglial activation and lack of recovery from the clinical signs of EAE. In addition, the number of neutrophils negatively correlates with that of B-cells in the CSF of MS patients (78). G-CSF administration at the onset of clinical symptoms reduces EAE severity in SJL/J mice by inhibiting recruitment of T-cells to the CNS and suppressing TNF-α production (79). G-CSF administration on day 12 of classical EAE led to expansion of $Ly6G^{+}$ neutrophils and faster recovery from clinical symptoms than control treated mice (78). In contrast, studies that show a detrimental role for neutrophils, including our findings, typically used models that impaired neutrophil function throughout the course of EAE or starting before the pre-onset phase (20, 44, 48). Furthermore, there is complexity with respect to neutrophils and G-CSF, depending on the phenotype of EAE. Our findings are consistent with Pierson and Goverman (49), who demonstrated that neutrophils are not necessary for classical EAE. Regarding the role of G-CSF, Rumble et al., (20) demonstrated that mice lacking G-CSF signaling are resistant to classical EAE, utilizing mice with global G-CSFR deletion. In our model, anti-G-CSF Ab was administered on day 7 after immunization, and suppressed the brain-targeted atypical EAE phenotype while not influencing classical EAE. These differences may reflect the timing at which G-CSF signaling is interrupted. Collectively, these findings indicate that the biological functions of neutrophils in EAE are timing, context and model dependent, with both beneficial and detrimental behaviors (11-13, 15).

Our RNA-seq analysis identified numerous genes that are differentially expressed in *Socs3*-deficient neutrophils in response to G-CSF, as compared to $Socs3^{fl/fl}$ mice.

Although some of these genes are likely direct targets of STAT3 based on GSEA, the majorities are not. GSEA results implicate the NF-κB pathway as the most affected signaling pathway, with more than 150 NF-κB target genes upregulated in *Socs3*-deficient neutrophils in response to G-CSF compared to *Socs3*$^{fl/fl}$ mice. Previous studies have suggested that *Socs3* negatively regulates the NF-κB pathway in macrophages (80), and our data suggest that *Socs3* may also negatively regulate the NF-κB pathway in neutrophils. The RNA-seq data also demonstrate that the STAT5 pathway, which is activated by GM-CSF, is enhanced in *Socs3*-deficient neutrophils after an 8 h stimulation with G-CSF. G-CSF priming also rendered *Socs3*-deficient neutrophils more sensitive to GM-CSF treatment for ROS production. GM-CSF is an important cytokine implicated in EAE/MS (49, 72, 81-83). Our findings demonstrate that G-CSF priming of *Socs3*-deficient neutrophils, leading to hyper-activation of STAT3, render these cells more sensitive to GM-CSF stimulation. This may contribute, in part, to their detrimental functions. Another interesting finding from our RNA-seq results is that neutrophils undergo metabolic changes in response to G-CSF, specifically increased glycolysis and reduced oxidative phosphorylation. mTOR signaling and hypoxia-related genes were also upregulated after G-CSF treatment. Although the literature exploring the relationship between metabolism and neutrophil function is limited, activation of mTORC1 and hypoxia inducible factor-1α (HIF1-α) have been shown to correlate with neutrophil activation and increased potential to form NETs (84-86). Previous studies have also demonstrated that *Socs3*-deficient neutrophils exhibit reduced apoptosis, consistent with our RNA-seq results showing upregulation of anti-apoptotic pathways (37, 38). Overall, our RNA-seq analysis provides some potential down-stream signaling

pathways that may be involved in the hyper-activation of *Socs3*-deficient neutrophils, which will be characterized in the future.

Neutrophils are critically involved in the pathophysiology of numerous CNS diseases including MS, NMOSD, Alzheimer's Disease and cerebral ischemia (15, 25, 87-89). The findings from our study may have relevance to NMOSD in addition to MS, given the well-documented presence of neutrophils in CNS lesions and CSF, and findings that neutrophils contribute to astrocyte dysfunction and inflammation in NMOSD animal models (25, 26). Furthermore, neutrophils from NMOSD patients exhibit some characteristics of activated neutrophils, including increased expression of TLR2 and fMLP receptors (25). Thus, the *Socs3*$^{\Delta LysM}$ model with hyper-activated neutrophils may be of value in further studies of NMOSD pathophysiology. Finally, the composition of the gut microbiome has profound effects in MS and NMOSD pathogenesis (90-92). A role for the gut microbiome in regulating a disease-promoting, primed neutrophil phenotype has recently been described (51). It will be of interest to examine how modulation of the microbiota in *Socs3*$^{\Delta LysM}$ mice may affect neutrophil function and subsequent neuroinflammatory responses in the CNS.

Methods

Mice. C57BL/6 mice were bred in an animal facility at the University of Alabama at Birmingham (UAB). Transgenic mice with the *Socs3* locus flanked with flox sequences (*Socs3*$^{fl/fl}$; (93)) were the generous gift of Dr. Warren Alexander (Walter and Eliza Hall Institute of Medical Research; Victoria, Australia) and were bred at UAB. *Socs3* conditional knockout (*Socs3*$^{\Delta LysM}$) mice were generated by serial breeding of *Socs3*$^{fl/fl}$ mice with mice expressing Cre recombinase under control of the *LysM* promoter (45).

Experimental Autoimmune Encephalomyelitis (EAE) Induction and Assessment. EAE was induced in *Socs3*$^{fl/fl}$ mice and *Socs3*$^{\Delta LysM}$ mice by subcutaneous (s.c.) injection of $MOG_{35–55}$ emulsified in CFA (Hooke Laboratories, EK-2110) along with i.p. injection of 100 ng Pertussis Toxin (PTX, Hooke Laboratories, EK-2110) on Day 0 and Day 1, as previously described (44, 45, 94). Mice experience classical, atypical or a mixed phenotype after EAE induction. Classical EAE was scored as follows: 0, no disease; 1, decreased tail tone; 2, hind limb weakness or partial paralysis; 3, complete hind limb paralysis; 4, front and hind limb paralysis; and 5, moribund state. Assessment of atypical EAE was as follows: 0, no disease; 1, hunched appearance, slight head tilt; 2, ataxia, scruffy coat; 3, severe head tilt, slight axial rotation, staggered walking; 4, severe axial rotation, spinning; and 5, moribund. For the mixed phenotype, classical and atypical EAE were scored separately. For ROS scavenger treatment experiments, mice were administered either phosphate-buffered saline (PBS) containing 8% DMSO (vehicle) or a ROS scavenger cocktail, which includes 20 mg/kg of FeTPPS (Cayman Chemical), 50 mg/kg of PBN (Sigma-Aldrich) and 15 mg/kg of EUK-134 (Sigma-

Aldrich), by i.p. injection twice a day for 5-6 days (56). For G-CSF depletion, 20 μg of anti-G-CSF Ab (R&D, MAB414) or isotype control rat IgG1 Ab (R&D, MAB005) was administered per mouse every other day by i.p. injection from days 7 to 12 post-induction (95). Mice were sacrificed on days 13-14 at the peak of EAE development for histology or flow cytometry analysis.

Assessment of Demyelination. At the peak of EAE, mice were anesthetized and intracardially perfused with PBS, followed by 4% paraformaldehyde. The cerebellum was fixed with 4% PFA at 4°C overnight and then dehydrated with 30% sucrose. Cryoprotected brains were embedded in Optimal Cutting Temperature compound (Fisher Scientific) and cryosectioned to produce 40 μm slices in the sagittal plane from the center. Sections were stained using the Black Gold II Myelin Staining Kit (Millipore Sigma, AG105) (96). Images of stained sections were acquired with Keyence Microscope BZ-X800. Total *arbor vitae* (white matter) area and the myelinated area (area of black-gold staining) of the cerebellum were measured using the "Hybrid Cell Count" module provided by Keyence Microscope. "% of Myelinated Area" was defined as myelinated area divided by total *arbor vitae* (white matter) area.

Antibodies, Cytokines and Inhibitors. For flow cytometry related experiments, antibodies (Abs) directed against murine CD11b (M1/70), CD45 (30-F11), Ly6C (HK1.4), Ly6G (1A8), CXCR2 (SA044G4), CD62L (MEL-14), CD63 (NVG-2), CD3 (17A2), CD4 (GK1.5), CD8 (53-6.7), CD44 (IM7), IFN-γ (XMG1.2) and IL-17A (TC11-18H10.1) were from BioLegend. Abs against GM-CSF (MP1-22E9) and Foxp3 (FJK-16S) were from

eBioscience. Tetramer Ab against MOG_{38-49} (GWYRSPFSRVVH) was a generous gift from Dr. Laurie Harrington (UAB). Abs against CXCR4 (2B11) was purchased from BD Bioscience, and Ab directed against pSTAT3 (Tyr705) was purchased from Cell Signaling Technology. The LIVE/DEAD® Fixable Aqua Stain kit was from Thermo Fisher (L34957). Murine IL-6, IFN-γ, G-CSF, sIL-6R, IL-23, TNF-α and GM-CSF were purchased from Biolegend. Neutralizing anti-G-CSF Ab was from R&D. AZD1480, a JAK1/2 inhibitor, was a generous gift from AstraZeneca R&D (Waltham, MA) and dissolved in DMSO as previously described (31). PF8041, a JAK1 inhibitor, was provided by Pfizer (Cambridge, MA) and dissolved in DMSO.

Neutrophil Isolation. Bone marrow cells were isolated from the femurs of C57BL/6, *Socs3*$^{fl/fl}$ or *Socs3*$^{\Delta LysM}$ mice as previously described (36, 44). Red blood cells were lysed by incubation in ACK lysis buffer for 1 min. $CD45^+CD11b^+Ly6G^+$ neutrophils were isolated by flow cytometry and used for quantitative reverse transcriptase-polymerase chain reaction (qRT-PCR) assays. For functional assays, neutrophils were isolated using the negative selection procedure from the EasySep™ mouse neutrophil enrichment kit (Stemcell Biotechnologies).

Quantitative RT-PCR and RNA-sequencing (RNA-seq). Neutrophils isolated by flow cytometry were stimulated as indicated. Total RNA was purified from cells using Trizol reagent extraction, and 500 ng–2 µg of RNA was sent to GENEWIZ (South Plainfield, NJ) for RNA-seq and bioinformatics analysis. RNA-seq results were submitted to the National Center for Biotechnology Information Gene Expression Omnibus for archiving

under accession number (GSE122353). For generation of the heatmap, all significantly regulated genes were used. For other analysis, an FDR < 0.05 with more than a 1.5 fold change was considered as differentially expressed genes (DEGs). Genes with normalized count below 50 were removed from the list to ensure the quality of DEGs. Pathway analysis was performed using the Gene Set Enrichment Analysis (GSEA) program available from the Broad Institute. For qRT-PCR analysis, 500-1000 ng of RNA was used as a template for cDNA synthesis. qRT-PCR was performed using TaqMan primers purchased from Thermo Fisher Scientific. The resulting data were analyzed using the comparative cycle threshold method to calculate relative RNA quantities (94).

Flow Cytometry. For surface protein detection, cells were incubated with Fc Block (2.4G2) for 15 min and washed, followed by incubation with viability dye and the indicated Abs directed against cell surface proteins. CM-H2DCFDA, a general oxidative stress indicator, was used to detect total ROS production (18, 56). Cells were incubated with 1 μM CM-H2DCFDA (Thermo Fisher, C6827) at 37°C for 30 min, followed by staining of surface proteins as described above. To detect NOX2-mediated superoxide production, cells were incubated with Dihydroethidium (DHE) (Thermo Fisher, D11347) on ice for 30 min., and surface staining was performed simultaneously (97). Fluorescence levels were analyzed by flow cytometry within 6 h of staining without fixation. For intracellular cytokine staining, cells were stimulated with PMA (25 ng/ml) and ionomycin (1 μg/ml) in the presence of GolgiStop (BD Biosciences) for 4 h and were permeabilized using the Foxp3 Staining Buffer Kit (eBioscience), as previously

described (98). For MOG tetramer staining, cells were stained with tetramer at 37°C for 60 min (99).

To analyze levels of phospho-STAT3, cells were stimulated with various cytokines for the indicated times, and then fixed with BD Phosflow Lyse/Fix Buffer (BD, 558049) immediately after stimulation at 37°C for 10 min. Cells were then permeabilized with pre-chilled BD Phosflow Perm buffer III (BD, 558050) on ice for 30 min., followed by staining for phospho-STAT3 for 1 h. Stained cells were analyzed by flow cytometry immediately after staining.

For analysis of cells from the *in vivo* EAE experiments, mice were sacrificed and whole body perfusion was performed. Mononuclear cells were isolated from the cerebellum using a 30%/70% Percoll (GE Healthcare, 17089101) gradient. Cell phenotypes were determined based on surface and intracellular staining patterns analyzed by flow cytometry, as previously described (31, 45). All flow cytometry data was analyzed using FlowJo software (TreeStar).

Luminol Assay. Bone marrow neutrophils were incubated with G-CSF (10 ng/ml) for 12 h, transferred to 96-well plates (2-5 x 10^5 cells per well), and washed with HBSS medium. Neutrophils were incubated with PMA (Sigma Aldrich, P1585) (10 ng/ml), the cytokine of interest, luminol (Sigma Aldrich, 123072) (200 nM), and horseradish peroxidase (HRP, Sigma Aldrich, P8375) (1.6 units/ml). Luminescence was measured immediately thereafter and every 2 min for 60 min (100).

Statistics. Significant differences between two groups were analyzed by Student's *t*-test distribution. One-way ANOVA was used to compare differences between more than two samples, and the Mann-Whitney rank sum test was used for EAE scores. *P*-values less than 0.05 were considered statistically significant. All error bars represent standard error of the mean (SEM).

Study Approval. All animal experiments were reviewed and approved by the Institutional Animal Care and Use Committee of UAB.

Author contributions

Z.Y., H.Q. and E.N.B. designed and analyzed the experiments. Z.Y., W.Y., S.A.G., K.L., L.P., H.W. and F.C. performed the experiments. Z.Y., H.Q. and E.N.B. wrote the manuscript. J.S.D. helped design and interpret experiments related to ROS detection. A.S.W. and W.C. assisted with RNA-seq data analysis.

Acknowledgements

This work was supported by National Institutes of Health Grants R01NS057563 (to E.N.B.), R01AI061061 (to A.S.W.), and R01HL128502 (to J.S.D.) and National Multiple Sclerosis Society Grant RG-1606-24794 (to H.Q.). The Comprehensive Flow Cytometry Core at University of Alabama at Birmingham is supported by National Institutes of Health Grants P30 AR048311 and P30 AI27667. We thank Dr. Hubert Tse (UAB) and lab members for their assistance with the Luminol assay. We thank Dr. Laurie Harrington (UAB) for the reagents and assistance with tetramer staining.

References

1. Dendrou CA, Fugger L, and Friese MA. Immunopathology of multiple sclerosis. *Nat Rev Immunol.* 2015;15(9):545-58.
2. Reich DS, Lucchinetti CF, and Calabresi PA. Multiple sclerosis. *N Engl J Med.* 2018;378(2):169-80.
3. Thompson AJ, Baranzini SE, Geurts J, Hemmer B, and Ciccarelli O. Multiple sclerosis. *Lancet.* 2018;391(10130):1622-36.
4. Hemmer B, Kerschensteiner M, and Korn T. Role of the innate and adaptive immune responses in the course of multiple sclerosis. *Lancet Neurol.* 2015;14(4):406-19.
5. Robinson AP, Harp CT, Noronha A, and Miller SD. The experimental autoimmune encephalomyelitis (EAE) model of MS: utility for understanding disease pathophysiology and treatment. *Handb Clin Neurol.* 2014;122:173-89.
6. Nicolas-Avila JA, Adrover JM, and Hidalgo A. Neutrophils in homeostasis, immunity, and cancer. *Immunity.* 2017;46(1):15-28.
7. Wang J, Hossain M, Thanabalasuriar A, Gunzer M, Meininger C, and Kubes P. Visualizing the function and fate of neutrophils in sterile injury and repair. *Science.* 2017;358(6359):111-6.
8. Mayadas TN, Cullere X, and Lowell CA. The multifaceted functions of neutrophils. *Annu Rev Pathol.* 2014;9:181-218.
9. Nauseef WM, and Borregaard N. Neutrophils at work. *Nat Immunol.* 2014;15(7):602-11.
10. Soehnlein O, Steffens S, Hidalgo A, and Weber C. Neutrophils as protagonists and targets in chronic inflammation. *Nat Rev Immunol.* 2017;17(4):248-61.
11. Pierson ER, Wagner CA, and Goverman JM. The contribution of neutrophils to CNS autoimmunity. *Clin Immunol.* 2018;189:23-8.
12. Casserly CS, Nantes JC, Whittaker Hawkins RF, and Vallieres L. Neutrophil perversion in demyelinating autoimmune diseases: Mechanisms to medicine. *Autoimmun Rev.* 2017;16(3):294-307.
13. Miller NM, Wang J, Tan Y, and Dittel BN. Anti-inflammatory mechanisms of IFN-gamma studied in experimental autoimmune encephalomyelitis reveal neutrophils as a potential target in multiple sclerosis. *Front Neurosci.* 2015;9:287.
14. Saadoun S, et al. Neutrophil protease inhibition reduces neuromyelitis optica-immunoglobulin G-induced damage in mouse brain. *Ann Neurol.* 2012;71(3):323-33.
15. Woodberry T, Bouffler SE, Wilson AS, Buckland RL, and Brustle A. The emerging role of neutrophil granulocytes in multiple sclerosis. *J Clin Med.* 2018;7(12):511.
16. Lévesque SA, et al. Myeloid cell transmigration across the CNS vasculature triggers IL-1β–driven neuroinflammation during autoimmune encephalomyelitis in mice. *J Exp Med.* 2016; 213(6):929-49.
17. Jiang W, St-Pierre S, Roy P, Morley BJ, Hao J, and Simard AR. Infiltration of $CCR2^{+}Ly6C^{high}$ proinflammatory monocytes and neutrophils into the central nervous system is modulated by nicotinic acetylcholine receptors in a model of multiple sclerosis. *J Immunol.* 2016;196(5):2095-108.

18. Steinbach K, Piedavent M, Bauer S, Neumann JT, and Friese MA. Neutrophils amplify autoimmune central nervous system infiltrates by maturing local APCs. *J Immunol.* 2013;191(9):4531-9.
19. Aube B, et al. Neutrophils mediate blood-spinal cord barrier disruption in demyelinating neuroinflammatory diseases. *J Immunol.* 2014;193(5):2438-54.
20. Rumble JM, et al. Neutrophil-related factors as biomarkers in EAE and MS. *J Exp Med.* 2015;212(1):23-35.
21. Naegele M, Tillack K, Reinhardt S, Schippling S, Martin R, and Sospedra M. Neutrophils in multiple sclerosis are characterized by a primed phenotype. *J Neuroimmunol.* 2012;242(1-2):60-71.
22. Openshaw H, et al. Multiple sclerosis flares associated with recombinant granulocyte colony-stimulating factor. *Neurology.* 2000;54(11):2147-50.
23. Rust H, Kuhle J, Kappos L, and Derfuss T. Severe exacerbation of relapsing-remitting multiple sclerosis after G-CSF therapy. *Neurol Neuroimmunol Neuroinflamm.* 2016;3(2):e215.
24. Wingerchuk DM, et al. International consensus diagnostic criteria for neuromyelitis optica spectrum disorders. *Neurology.* 2015;85(2):177-89.
25. Hertwig L, et al. Distinct functionality of neutrophils in multiple sclerosis and neuromyelitis optica. *Mult Scler.* 2016;22(2):160-73.
26. Piatek P, et al. C5a-preactivated neutrophils are critical for autoimmune-induced astrocyte dysregulation in neuromyelitis optica spectrum disorder. *Front Immunol.* 2018;9:1694.
27. Jacob A, et al. Detrimental role of granulocyte-colony stimulating factor in neuromyelitis optica: clinical case and histological evidence. *Mult Scler.* 2012;18(12):1801-3.
28. Villarino AV, Kanno Y, and O'Shea JJ. Mechanisms and consequences of Jak-STAT signaling in the immune system. *Nat Immunol.* 2017;18(4):374-84.
29. O'Shea JJ, Schwartz DM, Villarino AV, Gadina M, McInnes IB, and Laurence A. The JAK-STAT pathway: Impact on human disease and therapeutic intervention. *Annu Rev Med.* 2015;66:311-28.
30. Yan Z, Gibson SA, Buckley JA, Qin H, and Benveniste EN. Role of the JAK/STAT signaling pathway in regulation of innate immunity in neuroinflammatory diseases. *Clin Immunol.* 2018;189:4-13.
31. Liu Y, et al. Therapeutic efficacy of suppressing the JAK/STAT pathway in multiple models of experimental autoimmune encephalomyelitis. *J Immunol.* 2014;192:59-72.
32. Cenit MC, et al. STAT3 locus in inflammatory bowel disease and multiple sclerosis susceptibility. *Genes Immun.* 2010;11(3):264-8.
33. Jakkula E, et al. Genome-wide association study in a high-risk isolate for multiple sclerosis reveals associated variants in STAT3 gene. *Am J Hum Gen.* 2010;86(2):285-91.
34. Frisullo G, et al. pSTAT1, pSTAT3, and T-bet expression in peripheral blood mononuclear cells from relapsing-remitting multiple sclerosis patients correlates with disease activity. *J Neurosci Res.* 2006;84(5):1027-36.
35. Croker BA, Kiu H, and Nicholson SE. SOCS regulation of the JAK/STAT signalling pathway. *Semin Cell Dev Biol.* 2008;19(4):414-22.

36. Qin H, Holdbrooks AT, Liu Y, Reynolds SL, Yanagisawa LL, and Benveniste EN. SOCS3 deficiency promotes M1 macrophage polarization and inflammation. *J Immunol.* 2012;189(7):3439-48.
37. Croker BA, et al. SOCS3 is a critical physiological negative regulator of G-CSF signaling and emergency granulopoiesis. *Immunity.* 2004;20(2):153-65.
38. Kimura A, et al. SOCS3 is a physiological negative regulator for granulopoiesis and granulocyte colony-stimulating factor receptor signaling. *J Biol Chem.* 2004;279(8):6905-10.
39. Frisullo G, et al. The effect of disease activity on leptin, leptin receptor and suppressor of cytokine signalling-3 expression in relapsing-remitting multiple sclerosis. *J Neuroimmunol.* 2007;192(1-2):174-83.
40. Araki M, et al. Efficacy of the anti-IL-6 receptor antibody tocilizumab in neuromyelitis optica: a pilot study. *Neurology.* 2014;82(15):1302-6.
41. Lin J, Li X, and Xia J. Th17 cells in neuromyelitis optica spectrum disorder: a review. *Int J Neurosci.* 2016;126(12):1051-60.
42. Barros PO, et al. Prediction of disease severity in neuromyelitis optica by the levels of interleukin (IL)-6 produced during remission phase. *Clin Exp Immunol.* 2016;183(3):480-9.
43. DuPage M, and Bluestone JA. Harnessing the plasticity of CD4(+) T cells to treat immune-mediated disease. *Nat Rev Immunol.* 2016;16(3):149-63.
44. Liu Y, Holdbrooks AT, Meares GP, Buckley JA, Benveniste EN, and Qin H. Preferential recruitment of neutrophils into the cerebellum and brainstem contributes to the atypical experimental autoimmune encephalomyelitis phenotype. *J Immunol.* 2015;195(3):841-52.
45. Qin H, et al. Signal transducer and activator of transcription-3/suppressor of cytokine signaling-3 (STAT3/SOCS3) axis in myeloid cells regulates neuroinflammation. *Proc Natl Acad Sci U S A.* 2012;109(13):5004-9.
46. Hawkins RFW, et al. ICAM1+ neutrophils promote chronic inflammation via ASPRV1 in B cell-dependent autoimmune encephalomyelitis. *JCI Insight.* 2017;2(23):e96882.
47. Marro BS, Grist JJ, and Lane TE. Inducible expression of CXCL1 within the central nervous system amplifies viral-induced demyelination. *J Immunol.* 2016;196(4):1855-64.
48. Simmons SB, Liggitt D, and Goverman JM. Cytokine-regulated neutrophil recruitment is required for brain but not spinal cord inflammation during experimental autoimmune encephalomyelitis. *J Immunol.* 2014;193(2):555-63.
49. Pierson ER, and Goverman JM. GM-CSF is not essential for experimental autoimmune encephalomyelitis but promotes brain-targeted disease. *JCI Insight.* 2017;2(7):e92362.
50. Stoolman JS, et al. An IFNgamma/CXCL2 regulatory pathway determines lesion localization during EAE. *J Neuroinflammation.* 2018;15(1):208.
51. Zhang D, et al. Neutrophil ageing is regulated by the microbiome. *Nature.* 2015;525(7570):528-32.
52. Silvestre-Roig C, Hidalgo A, and Soehnlein O. Neutrophil heterogeneity: implications for homeostasis and pathogenesis. *Blood.* 2016;127(18):2173-81.

53. Reber LL, et al. Neutrophil myeloperoxidase diminishes the toxic effects and mortality induced by lipopolysaccharide. *J Exp Med.* 2017;214(5):1249-58.
54. Wright HL, Moots RJ, and Edwards SW. The multifactorial role of neutrophils in rheumatoid arthritis. *Nat Rev Rheumatol.* 2014;10(10):593-601.
55. Martin-Martin B, Nabokina SM, Blasi J, Lazo PA, and Mollinedo F. Involvement of SNAP-23 and syntaxin 6 in human neutrophil exocytosis. *Blood.* 2000;96(7):2574-83.
56. Noubade R, et al. NRROS negatively regulates reactive oxygen species during host defence and autoimmunity. *Nature.* 2014;509(7499):235-9.
57. Kim K, Li J, Tseng A, Andrews RK, and Cho J. NOX2 is critical for heterotypic neutrophil-platelet interactions during vascular inflammation. *Blood.* 2015;126(16):1952-64.
58. Park L, Anrather J, Girouard H, Zhou P, and Iadecola C. Nox2-derived reactive oxygen species mediate neurovascular dysregulation in the aging mouse brain. *J Cereb Blood Flow Metab.* 2007;27(12):1908-18.
59. Cooney SJ, Bermudez-Sabogal SL, and Byrnes KR. Cellular and temporal expression of NADPH oxidase (NOX) isotypes after brain injury. *J Neuroinflammation.* 2013;10:155.
60. Broggi A, Tan Y, Granucci F, and Zanoni I. IFN-lambda suppresses intestinal inflammation by non-translational regulation of neutrophil function. *Nat Immunol.* 2017;18(10):1084-93.
61. Rottenberg ME, and Carow B. SOCS3, a major regulator of infection and inflammation. *Front Immunol.* 2014;5:58.
62. Nguyen-Jackson H, Panopoulos AD, Zhang H, Li HS, and Watowich SS. STAT3 controls the neutrophil migratory response to CXCR2 ligands by direct activation of G-CSF-induced CXCR2 expression and via modulation of CXCR2 signal transduction. *Blood.* 2010;115(16):3354-63.
63. Zhang H, Nguyen-Jackson H, Panopoulos AD, Li HS, Murray PJ, and Watowich SS. STAT3 controls myeloid progenitor growth during emergency granulopoiesis. *Blood.* 2010;116(14):2462-71.
64. Panopoulos AD, et al. STAT3 governs distinct pathways in emergency granulopoiesis and mature neutrophils. *Blood.* 2006;108(12):3682-90.
65. Taylor PR, et al. Activation of neutrophils by autocrine IL-17A-IL-17RC interactions during fungal infection is regulated by IL-6, IL-23, RORgammat and dectin-2. *Nat Immunol.* 2014;15(2):143-51.
66. Wilkinson AN, et al. Granulocytes are unresponsive to IL-6 due to an absence of gp130. *J Immunol.* 2018;200(10):3547-55.
67. McDonald PP, Bald A, and Cassatella MA. Activation of the NF-kappaB pathway by inflammatory stimuli in human neutrophils. *Blood.* 1997;89(9):3421-33.
68. Kimura A, et al. The transcription factors STAT5A/B regulate GM-CSF-mediated granulopoiesis. *Blood.* 2009;114(21):4721-8.
69. Schwartz JT, et al. Francisella tularensis alters human neutrophil gene expression: insights into the molecular basis of delayed neutrophil apoptosis. *J Innate Immun.* 2013;5(2):124-36.

70. Hutchins AP, Takahashi Y, and Miranda-Saavedra D. Genomic analysis of LPS-stimulated myeloid cells identifies a common pro-inflammatory response but divergent IL-10 anti-inflammatory responses. *Sci Rep.* 2015;5:9100.
71. Sayed BA, Christy AL, Walker ME, and Brown MA. Meningeal mast cells affect early T cell central nervous system infiltration and blood-brain barrier integrity through TNF: a role for neutrophil recruitment? *J Immunol.* 2010;184(12):6891-900.
72. Spath S, et al. Dysregulation of the cytokine GM-CSF induces spontaneous phagocyte invasion and immunopathology in the central nervous system. *Immunity.* 2017;46(2):245-60.
73. Quintana A, et al. Site-specific production of IL-6 in the central nervous system retargets and enhances the inflammatory response in experimental autoimmune encephalomyelitis. *J Immunol.* 2009;183(3):2079-88.
74. Wensky AK, et al. IFN-gamma determines distinct clinical outcomes in autoimmune encephalomyelitis. *J Immunol.* 2005;174(3):1416-23.
75. Takashima A, and Yao Y. Neutrophil plasticity: acquisition of phenotype and functionality of antigen-presenting cell. *J Leukoc Biol.* 2015;98(4):489-96.
76. Evrard M, et al. Developmental analysis of bone marrow neutrophils reveals populations specialized in expansion, trafficking, and effector functions. *Immunity.* 2018;48(2):364-79.e8.
77. Grist JJ, et al. Induced CNS expression of CXCL1 augments neurologic disease in a murine model of multiple sclerosis via enhanced neutrophil recruitment. *Eur J Immunol.* 2018;48(7):1199-210.
78. Knier B, et al. Myeloid-derived suppressor cells control B cell accumulation in the central nervous system during autoimmunity. *Nat Immunol.* 2018;19(12):1341-51.
79. Zavala F, Abad S, Ezine S, Taupin V, Masson A, and Bach JF. G-CSF therapy of ongoing experimental allergic encephalomyelitis via chemokine- and cytokine-based immune deviation. *J Immunol.* 2002;168(4):2011-9.
80. Zhang X, et al. Macrophage/microglial Ezh2 facilitates autoimmune inflammation through inhibition of Socs3. *J Exp Med.* 2018; 215(5):1365-82.
81. Codarri L, et al. RORgammat drives production of the cytokine GM-CSF in helper T cells, which is essential for the effector phase of autoimmune neuroinflammation. *Nat Immunol.* 2011;12(6):560-7.
82. Croxford AL, Spath S, and Becher B. GM-CSF in neuroinflammation: licensing myeloid cells for tissue damage. *Trends Immunol.* 2015;36(10):651-62.
83. Duncker PC, Stoolman JS, Huber AK, and Segal BM. GM-CSF promotes chronic disability in experimental autoimmune encephalomyelitis by altering the composition of central nervous system-infiltrating cells, but is dispensable for disease induction. *J Immunol.* 2018;200(3):966-73.
84. Weichhart T, Hengstschlager M, and Linke M. Regulation of innate immune cell function by mTOR. *Nat Rev Immunol.* 2015;15(10):599-614.
85. Bao Y, et al. mTOR and differential activation of mitochondria orchestrate neutrophil chemotaxis. *J Cell Biol.* 2015;210(7):1153-64.
86. McInturff AM, et al. Mammalian target of rapamycin regulates neutrophil extracellular trap formation via induction of hypoxia-inducible factor 1 alpha. *Blood.* 2012;120(15):3118-25.

87. Strecker JK, Schmidt A, Schabitz WR, and Minnerup J. Neutrophil granulocytes in cerebral ischemia - Evolution from killers to key players. *Neurochem Int.* 2017;107:117-26.
88. Cruz Hernandez JC, et al. Neutrophil adhesion in brain capillaries reduces cortical blood flow and impairs memory function in Alzheimer's disease mouse models. *Nat Neurosci.* 2019;22(3):413-20.
89. Zenaro E, et al. Neutrophils promote Alzheimer's disease-like pathology and cognitive decline via LFA-1 integrin. *Nat Med.* 2015;21(8):880-6.
90. Cignarella F, et al. Intermittent fasting confers protection in CNS autoimmunity by altering the gut microbiota. *Cell Metab.* 2018;27(6):1222-35.e6.
91. Cree BA, Spencer CM, Varrin-Doyer M, Baranzini SE, and Zamvil SS. Gut microbiome analysis in neuromyelitis optica reveals overabundance of Clostridium perfringens. *Ann Neurol.* 2016;80(3):443-7.
92. Cekanaviciute E, et al. Gut bacteria from multiple sclerosis patients modulate human T cells and exacerbate symptoms in mouse models. *Proc Natl Acad Sci U S A.* 2017;114(40):10713-18.
93. Croker BA, et al. SOCS3 negatively regulates IL-6 signaling *in vivo*. *Nat Immunol.* 2003;4(6):540-5.
94. Gibson SA, et al. Protein kinase CK2 controls the fate between Th17 cell and regulatory T cell differentiation. *J Immunol.* 2017;198:4244-54.
95. Campbell IK, et al. Therapeutic targeting of the G-CSF receptor reduces neutrophil trafficking and joint inflammation in antibody-mediated inflammatory arthritis. *J Immunol.* 2016;197(11):4392-402.
96. Liu L, et al. CXCR2-positive neutrophils are essential for cuprizone-induced demyelination: relevance to multiple sclerosis. *Nat Neurosci.* 2010;13(3):319-26.
97. Anderson JT, et al. Elevated levels of NO are localized to distal airways in asthma. *Free Radic Biol Med.* 2011;50(11):1679-88.
98. Gibson SA, Yang W, Yan Z, Qin H, and Benveniste EN. CK2 controls Th17 and regulatory T cell differentiation through inhibition of FoxO1. *J Immunol.* 2018;201(2):383-92.
99. Tian Y, Mollo SB, Harrington LE, and Zajac AJ. IL-10 regulates memory T Cell development and the balance between Th1 and follicular Th cell responses during an acute viral infection. *J Immunol.* 2016;197(4):1308-21.
100. Padgett LE, and Tse HM. NADPH oxidase-derived superoxide provides a third signal for CD4 T cell effector responses. *J Immunol.* 2016;197(5):1733-42.

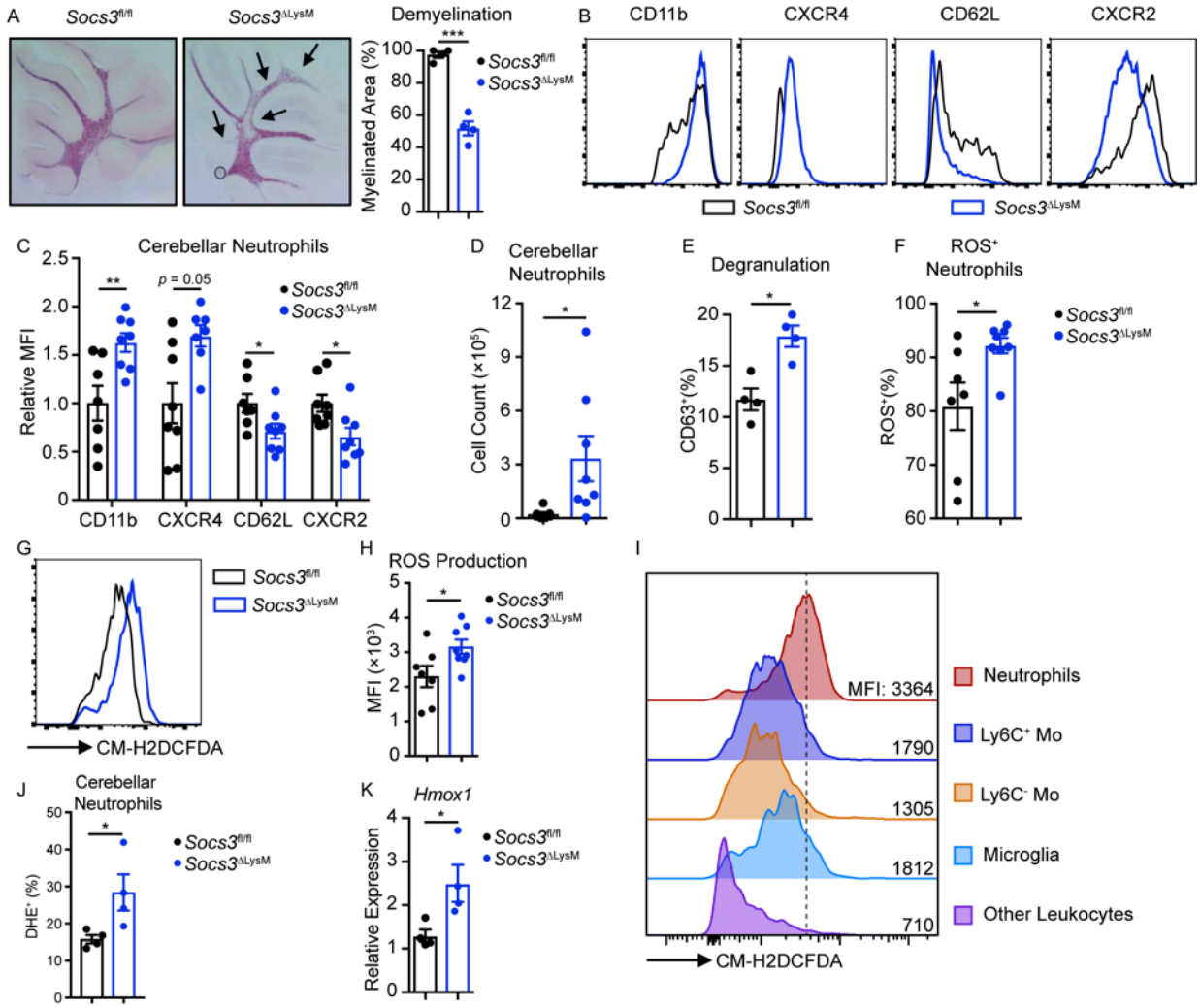

Figure 1. *Socs3*$^{\Delta LysM}$ Mice Exhibit Brain-targeted Atypical EAE with Infiltration of Hyper-activated Neutrophils. EAE was induced in both *Socs3*$^{fl/fl}$ and *Socs3*$^{\Delta LysM}$ mice, and cerebellar tissue collected at peak of disease for further analysis. **(A)** Demyelination was assessed at day 14 and quantified by Black Gold staining (n = 4). Arrows indicate demyelinated regions. **(B-J)** Immune cells isolated from the cerebellum at days 13-14 using a Percoll gradient were subjected to surface staining. **(B)** Overlay of cerebellar-infiltrating neutrophils from *Socs3*$^{fl/fl}$ and *Socs3*$^{\Delta LysM}$ mice stained for CD11b, CXCR4, CD62L and CXCR2 (n = 7-8). **(C)** Relative expression of surface markers of cerebellar-infiltrating neutrophils (n = 7-8). **(D)** Total number of cerebellar-infiltrating neutrophils (n = 7-8). **(E)** Degranulation was measured by analyzing the percentage of CD63$^+$ neutrophils at days 13-14 (n = 4). **(F-I)** Prior to surface staining, isolated neutrophils were incubated with CM-H2DCFDA (1 µM) at 37°C for 30 min. **(F)** Percentage of ROS-producing neutrophils (n = 7-8). **(G, H)** ROS production by neutrophils measured as the MFI of CM-H2DCFDA staining (n = 7-8). **(I)** ROS production by different immune cell types from the cerebellum at days 13-14. Neutrophils (CD45$^+$CD11b$^+$Ly6C^{lo}Ly6G$^+$); Ly6C$^+$ Monocytic Cells (Ly6C$^+$ Mo) (CD45$^+$CD11b$^+$Ly6C$^+$Ly6G$^-$); Ly6C$^-$ Monocytic Cells (Ly6C$^-$ Mo) (CD45$^+$CD11b$^+$ Ly6C$^-$Ly6G$^-$); Microglia (CD45^{lo}CD11b$^+$); and Other Leukocytes (CD45$^+$CD11b$^-$). Plot represents 8 individual samples. **(J)** Superoxide was measured using DHE (n = 4). **(K)** RNA was isolated from whole cerebellum at day 13, and *Hmox1* expression analyzed by qRT-PCR (n = 4). *p < 0.05, **p < 0.01, ***p < 0.001 by two-tailed Student's t test. MFI, mean fluorescent intensity; DHE, Dihydroethidium.

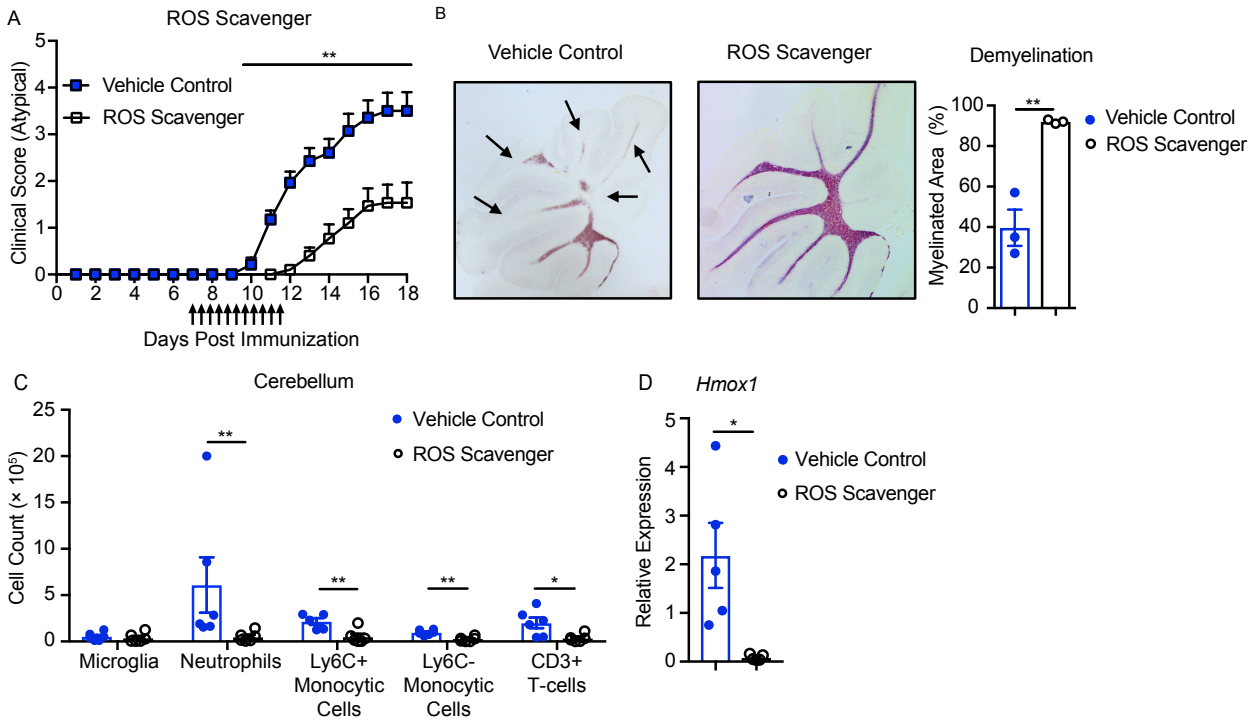

Figure 2. ROS Play an Important Role in the Pathology of Atypical EAE. EAE was induced in *Socs3*$^{\Delta LysM}$ mice. Beginning at day 7, ROS scavenger cocktail (FeTPPS 20 mg/kg, PBN 50 mg/kg and EUK134 15 mg/kg) was administered i.p. twice per day for 5 days. **(A)** Atypical EAE score of mice treated with ROS scavenger cocktail (n = 14) or vehicle control (n = 14). Mice that did not develop EAE (classical or atypical) were excluded. **(B)** Demyelination was assessed at day 14 and quantified by Black Gold staining (n = 3). Arrows indicate demyelinated regions. **(C)** At days 13-14, immune cells from the cerebellum were isolated by Percoll gradient, and the frequencies of Microglia ($CD45^{lo}CD11b^{+}$); Neutrophils ($CD45^{+}CD11b^{+}Ly6C^{lo}Ly6G^{+}$); $Ly6C^{+}$ Monocytic Cells ($CD45^{+}CD11b^{+}Ly6C^{+}Ly6G^{-}$); $Ly6C^{-}$ Monocytic Cells ($CD45^{+}CD11b^{+}Ly6C^{-}Ly6G^{-}$); and CD3+ T-cells ($CD45^{+}CD11b^{-}CD3^{+}$) were determined (n = 6). **(D)** RNA was isolated from whole cerebellum at day 13, and *Hmox1* expression analyzed by qRT-PCR (n = 5). $*p < 0.05$,$**p < 0.01$, by Mann-Whitney rank sum test **(A)** or two-tailed Student's t test **(B, C, D)**.

Table 1. ROS Scavengers Reduce the Incidence of Atypical EAE

Treatment	Overall Incidence	Classical[a]	Atypical[a]
Vehicle Control	14/14 (100%)	7/14 (50.0%)	13/14 (92.9%)
ROS Scavenger	14/17 (82.4%)	12/17 (70.5%)	8/17 (47.1%)**

[a]Incidence was calculated from all mice. **$p < 0.01$ with χ^2 test between Vehicle Control and ROS Scavenger groups.

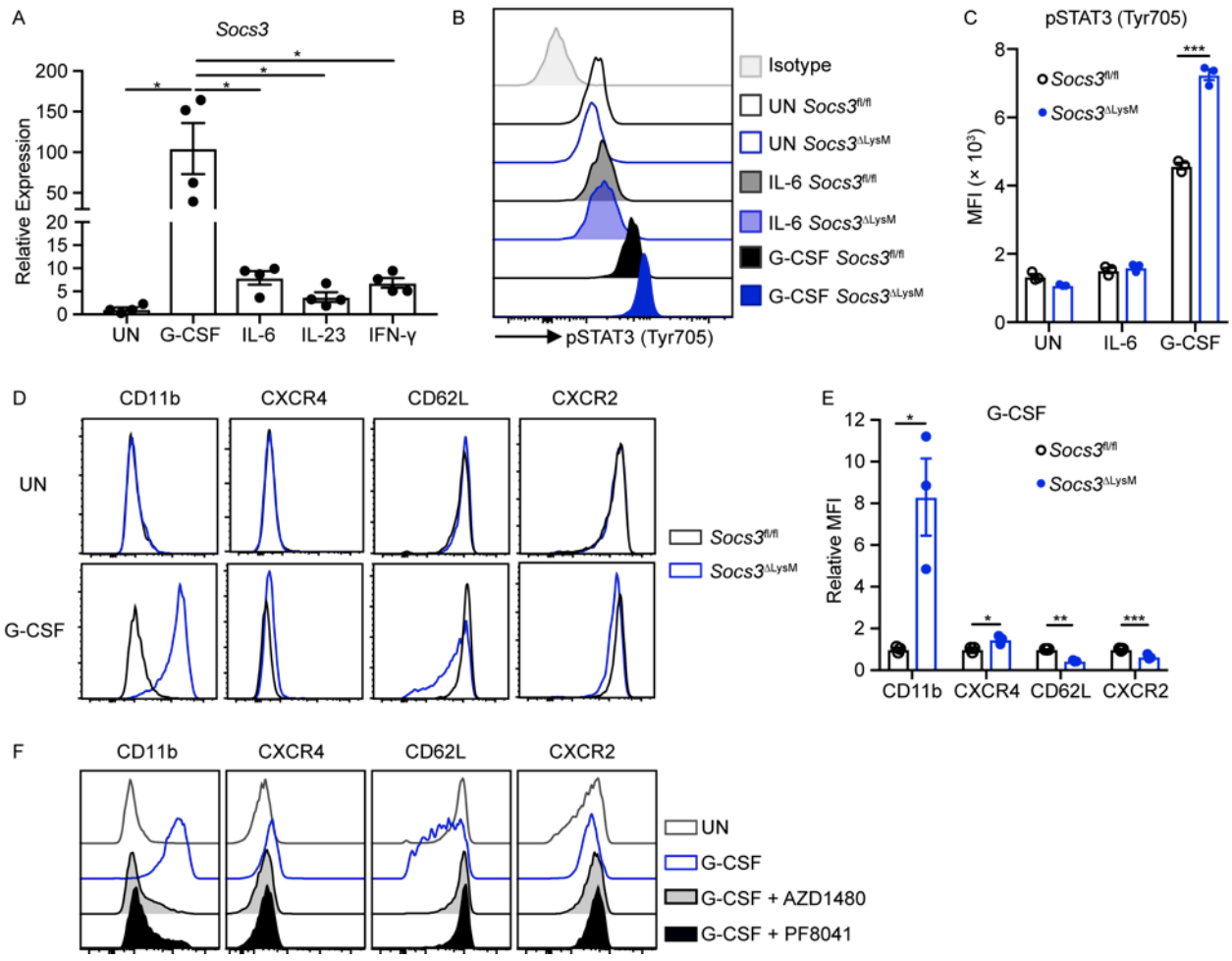

Figure 3. *Socs3* Deficiency Promotes G-CSF Hyper-sensitivity in Neutrophils via JAK1 Activation. **(A)** Bone marrow neutrophils were isolated from C57BL/6 mice and stimulated with G-CSF (10 ng/ml), IL-6 (100 ng/ml), IL-23 (10 ng/ml) or IFN-γ (10 ng/ml) for 2 h. Expression of *Socs3* mRNA was analyzed by qRT-PCR (n = 4). **(B-E)** Bone marrow neutrophils were isolated from $Socs3^{fl/fl}$ or $Socs3^{\Delta LysM}$ mice (n = 3). **(B, C)** Neutrophils were stimulated with G-CSF (10 ng/ml) or IL-6 (100 ng/ml) for 2 h followed by intracellular staining for pSTAT3 (Y705). **(D, E)** Neutrophils were stimulated with G-CSF (10 ng/ml) for 8 h, and expression of surface markers was analyzed. **(F)** Bone marrow neutrophils isolated from $Socs3^{\Delta LysM}$ mice were pre-treated with AZD1480 (25 μM) or PF8041 (25 μM) for 2 h and then stimulated with G-CSF (10 ng/ml) for 8 h, followed by surface staining. Plots are representative of three independent experiments. All flow cytometry plots **(B-F)** were gated on live, single $CD45^{+}CD11b^{+}Ly6G^{+}$ neutrophils. *$p < 0.05$, **$p < 0.01$, ***$p < 0.001$ by one-way ANOVA **(A)** or two-tailed Student's t test **(C, E)**. MFI, mean fluorescent intensity.

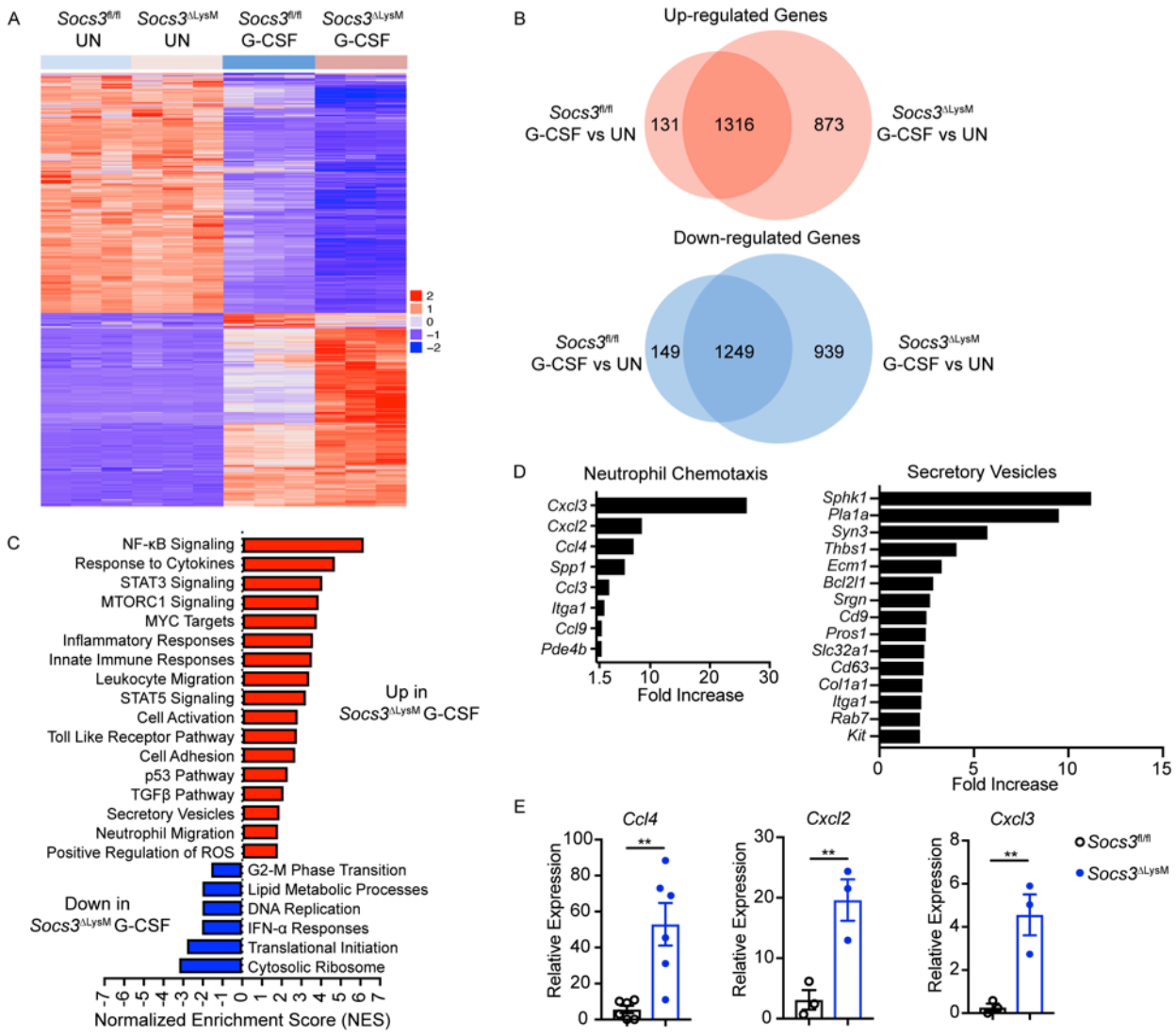

Figure 4. G-CSF Induces a Unique Gene Expression Profile in *Socs3*-deficient Neutrophils. Bone marrow neutrophils isolated from *Socs3*$^{fl/fl}$ and *Socs3*$^{\Delta LysM}$ mice were stimulated with G-CSF (10 ng/ml) for 8 h, followed by mRNA extraction and RNA-seq (n = 3). **(A)** Heatmap of differentially expressed genes among the four groups. **(B)** Venn diagram depicting differentially expressed genes between *Socs3*$^{fl/fl}$ and *Socs3*-deficient neutrophils in response to G-CSF. **(C)** Differentially expressed genes between *Socs3*-deficient neutrophils and *Socs3*$^{fl/fl}$ neutrophils upon G-CSF treatment were ranked based on the adjusted *p* value and Log2 fold change. Gene set enrichment analysis illustrating up- and down-regulated pathways in *Socs3*-deficient neutrophils in response to G-CSF. **(D)** Up-regulated genes from selected pathways. **(E)** Bone marrow neutrophils isolated from *Socs3*$^{fl/fl}$ and *Socs3*$^{\Delta LysM}$ mice were stimulated with G-CSF (10 ng/ml) for 8 h, followed by mRNA extraction and qPCR assay to determine mRNA expression of the indicated chemokines (n = 3-6). $^{**}p < 0.01$ by two-tailed Student's t test.

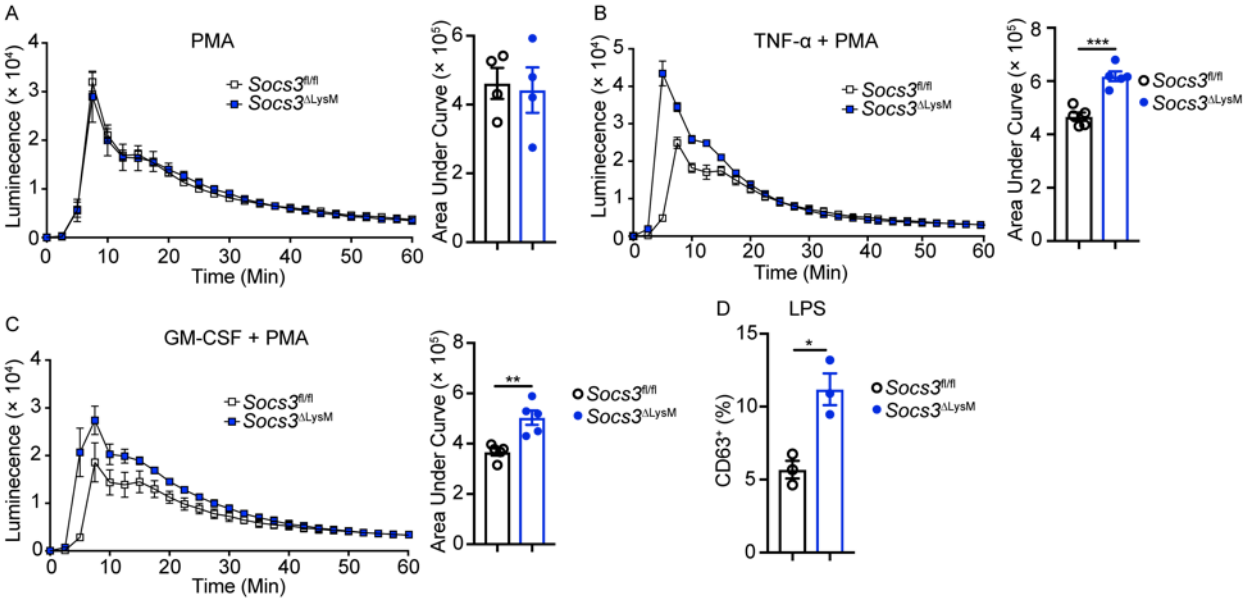

Figure 5. *Socs3*-deficient Neutrophils Are Functionally Hyper-activated *In Vitro* Upon G-CSF Priming. Bone marrow neutrophils were isolated from *Socs3*$^{fl/fl}$ or *Socs3*$^{\Delta LysM}$ mice and primed with G-CSF (10 ng/ml) for 12 h. **(A-C)** Neutrophils were incubated with PMA (10 ng/ml) **(A)**, **(B)** PMA plus TNF-α (10 ng/ml) or **(C)** PMA plus GM-CSF (10 ng/ml) and production of ROS was measured by a luminol assay. Plot represents 4-5 independent experiments. **(D)** G-CSF-primed neutrophils were stimulated with LPS (50 ng/ml) for 1 h, and degranulation determined by surface staining of CD63 (n = 3). Flow cytometry plots were gated on live, single CD45$^+$CD11b$^+$Ly6G$^+$ neutrophils. *p < 0.05, **p < 0.01, ***p < 0.001 by two-tailed Student's t test **(B-D)**.

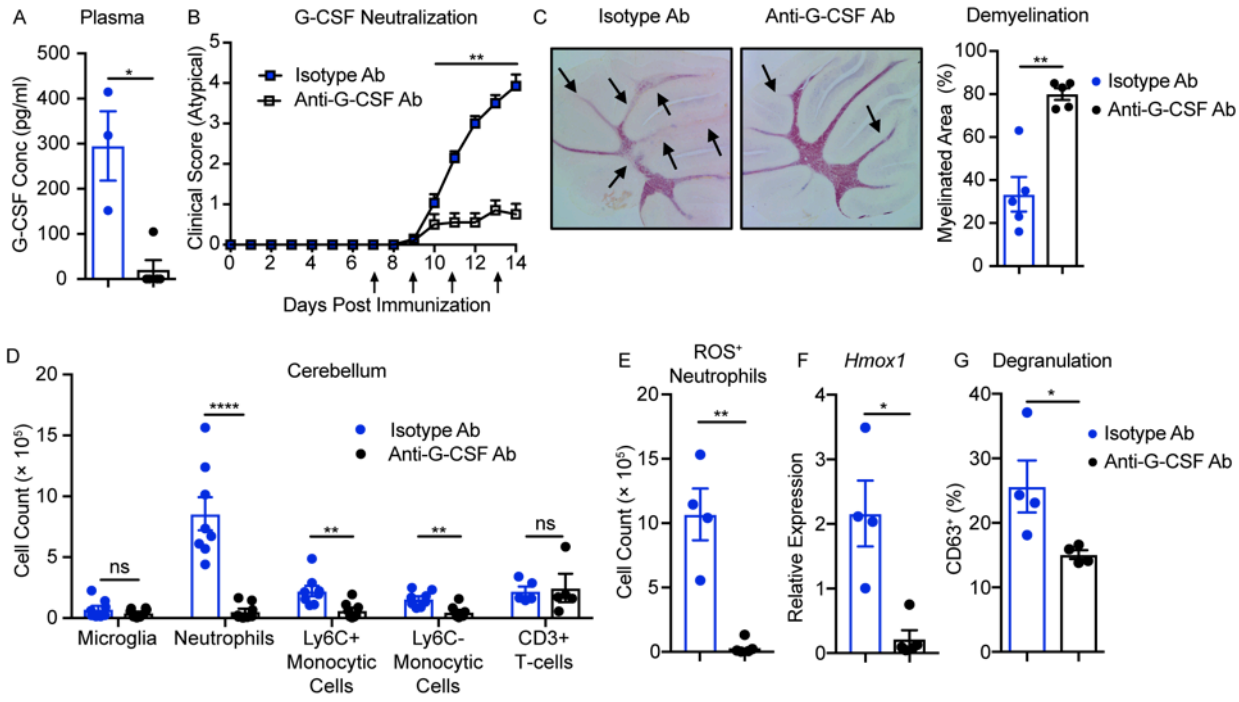

Figure 6. G-CSF Neutralization Suppresses Brain-targeted Atypical EAE. EAE was induced in *Socs3*$^{\Delta LysM}$ mice, and from day 7, anti-G-CSF Ab (20 µg/mouse) or isotype control Ab (20 µg/mouse) were administered i.p. every other day until day 13. **(A)** On day 12, plasma samples were collected and G-CSF levels determined by ELISA (n = 3). **(B)** Atypical EAE scoring of mice treated with anti-G-CSF Ab (n = 11) or isotype control Ab (n = 14). Mice that did not develop EAE (classical or atypical) were excluded. **(C)** Demyelination was assessed and quantified by Black Gold staining (n = 5). Arrows indicate demyelinated regions. **(D, E, G)** Immune cells were isolated from the cerebellum 14 days post-immunization (n = 5-8). **(D)** Frequencies of Microglia ($CD45^{lo}CD11b^{+}$); Neutrophils ($CD45^{+}CD11b^{+}Ly6C^{lo}Ly6G^{+}$); $Ly6C^{+}$ Monocytic Cells ($CD45^{+}CD11b^{+}Ly6C^{+}Ly6G^{-}$); $Ly6C^{-}$ Monocytic Cells ($CD45^{+}CD11b^{+}Ly6C^{-}Ly6G^{-}$); and CD3+ T-cells ($CD45^{+}CD11b^{-}CD3^{+}$) from the cerebella of isotype Ab and anti-G-CSF Ab-treated mice were determined. **(E)** Total numbers of ROS-producing neutrophils in the cerebella from isotype Ab and anti-G-CSF Ab-treated mice. **(F)** RNA was isolated from whole cerebellum, and *Hmox1* expression analyzed by qRT-PCR (n = 4). **(G)** Degranulation of cerebellar-infiltrating neutrophils from isotype Ab or anti-G-CSF Ab-treated mice was determined by surface expression of CD63. *$p < 0.05$, **$p < 0.01$, ****$p < 0.0001$, ns = not significant by Mann-Whitney rank sum test **(B)** or two-tailed Student's t test **(A, C-G)**.

Table 2. Anti-G-CSF Ab Reduces the Incidence of Atypical EAE

Treatment	Overall Incidence	Classical[a]	Atypical[a]
Isotype Ab	14/14 (100%)	8/14 (57.1%)	14/14 (100%)
Anti-G-CSF Ab	11/14 (78.6%)	7/14 (50.0%)	5/14 (35.7%)**

[a]Incidence was calculated from all mice. ** $p < 0.01$ with χ^2 test between anti-G-CSF Ab and Isotype Ab groups.